Gaussian Process-Enhanced, External and Internal Convertible Form-Based Control of Underactuated Balance Robots

Feng Han and Jingang Yi

Abstract—External and internal convertible (EIC) form-based motion control (i.e., EIC-based control) is one of the effective approaches for underactuated balance robots. By sequentially controller design, trajectory tracking of the actuated subsystem and balance of the unactuated subsystem can be achieved simultaneously. However, with certain conditions, there exists uncontrolled robot motion under the EIC-based control. We first identify these conditions and then propose an enhanced EIC-based control with a Gaussian process data-driven robot dynamic model. Under the new enhanced EIC-based control, the stability and performance of the closed-loop system are guaranteed. We demonstrate the GP-enhanced control experimentally using two examples of underactuated balance robots.

I. INTRODUCTION

An underactuated balance robot possesses fewer control inputs than the number of degrees of freedom (DOFs) [1], [2]. Control design of underactuated balance robots needs to achieve both the trajectory tracking of the actuated subsystem and balance control of the unactuated subsystem [3], [4]. The balance of unstable coordinates of underactuated robots brings additional challenges for robot control. Many methods have been proposed to cope with the robot modeling [1], [3]-[6], control design and applications [7], [8]. The external and internal convertible (EIC) form-based control (i.e., EIC-based control) has been demonstrated as one of the effective approaches to achieve simultaneous trajectory tracking and balance [9]. Other balance control algorithms include the orbital stabilization control [10]–[13], and energy shaping-based control [14]–[16]. One limitation of these methods is that the achieved balance-enforced trajectory is not unique [2], [17].

Although the EIC-based control achieves stability and balance [4], [9], [18], [19], certain system conditions should be satisfied. Furthermore, an accurate robot dynamics model is required and control robustness is not guaranteed under model uncertainties. Machine learning-based method provides an efficient tool for robot modeling and control. In particular, Gaussian process (GP) regression is an effective learning approach that generates analytical structure and bounded prediction errors [5], [20]–[23]. Development of GP-based performance-guaranteed control for underactuated balance robots has been reported [3], [20], [24], [25]. In [3], the control input is partitioned into two parts. A GP-based

This work was partially supported by the US National Science Foundation under award CNS-1932370.

F. Han and J. Yi are with the Department of Mechanical and Aerospace Engineering, Rutgers University, Piscataway, NJ 08854 USA (e-mail: fh233@scarletmail.rutgers.edu, jgyi@rutgers.edu).

inverse dynamics controller for unactuated subsystem to achieve balance and a model predictive control (MPC) design are used to simultaneously track the given reference trajectory and obtain the balance equilibrium manifold (BEM). The GP prediction uncertainties are incorporated into the control design to enhance the control robustness. The work in [4] followed the cascaded control design in the EIC-based framework and the controller was adaptive to the prediction uncertainties. The training data was also selected to reduce the computational complexity.

In this paper, we take advantage of the structured GP modeling in [4], [26] and present a method to resolve the limitation of the original EIC-based control. We first show that under EIC-based control, there exist uncontrolled motions that cause the entire system unstable. The uncontrolled motion is because the EIC-based control is updated from a low- to high-dimensional space. The conditions for the stable GP-based model learning and control are identified and presented. With the properly selected nominal model, the uncontrolled motion is eliminated with the GP-based data-driven robot dynamics. Finally, we propose a partial EIC (PEIC)-based control by constructing a virtual inertial matrix to reshape the dynamics coupling. The proposed GPbased control is shown to achieve guaranteed stability and performance. Experimental validation and demonstration are presented by using two underactuated balance robots.

The major contributions of this work are twofold. Compared with [4], [9], the uncontrolled motion of the EIC-based control is identified and illustrated. To overcome the identified EIC-based control limitations, the conditions for nominal GP model selection are presented. The proposed controller is new and also achieves good performance and stability. Second, unlike the work in [3] with the complex MPC with high computational cost, the proposed GP models directly capture the robot dynamics and the control design preserves the EIC structure property. The demonstrated experiments are also new compared with the previous work.

II. EIC-BASED CONTROL AND PROBLEM STATEMENT

A. Robot Dynamics and EIC-Based Control

We consider a general underactuated balance robot with (n+m) DOFs, $n,m \in \mathbb{N}$, and the generalized coordinates are denoted as $\mathbf{q} = [q_1 \cdots q_{n+m}]^T$. The dynamics model is expressed in a standard form

$$S: D(q)\ddot{q} + C(q, \dot{q})\dot{q} + G(q) = Bu, \tag{1}$$

where D(q), $C(q, \dot{q})$ and G(q) are the inertia, Coriolis and gravity matrices, respectively. B denotes the input matrix and $u \in \mathbb{R}^m$ is the control input.

The generalized coordinates are partitioned as $q = [q_a^T \ q_u^T]^T$, with actuated and unactuated coordinates $q_a \in \mathbb{R}^n$ and $q_u \in \mathbb{R}^m$, respectively. We focus on the case n > m. Without loss of generality, we assume that $B = [I_n \ 0]^T$, where $I_n \in \mathbb{R}^n$ is an identify matrix. The robot dynamics (1) is rewritten as

$$S_a: D_{aa}\ddot{q}_a + D_{au}\ddot{q}_u + H_a = u, \tag{2a}$$

$$S_u: D_{ua}\ddot{q}_a + D_{uu}\ddot{q}_u + H_u = 0 \tag{2b}$$

for actuated and unactuated subsystems, respectively. Subscripts "aa~(uu)" and "ua~ and au" indicate the variables related to the actuated (unactuated) coordinates and coupling effects, respectively. For representation convenience, we introduce $H=C\dot{q}+G,~H_a=C_a\dot{q}+G_a$, and $H_u=C_u\dot{q}+G_u$. The dependence of matrices D,~C,~ and G~ on q~ and $\dot{q}~$ is dropped. Subsystems $\mathcal{S}_a~$ and $\mathcal{S}_u~$ are referred to as external and internal subsystems, respectively [9].

Given the desired trajectory q_a^d the control input is first designed to follow q_a^d by temporarily neglecting S_u as

$$u^{\text{ext}} = D_{aa}v^{\text{ext}} + D_{au}\ddot{q}_u + H_a, \tag{3}$$

where error $e_a = q_a - q_a^d$ and $v^{\text{ext}} \in \mathbb{R}^n$ is the auxiliary input that drives e_a to the origin. To account for the dynamics coupling, q_u is balanced onto BEM. We note \mathcal{S}_u takes the motion effect \ddot{q}_a as an "external" control input. Assuming the designed control u^{ext} is applied to the system. The actuated coordinates display the dynamics $\ddot{q}_a = v^{\text{ext}}$. The BEM is defined as the instantaneous equilibrium of q_u under the "external" control. The BEM under control v^{ext} is

$$\mathcal{E} = \left\{ \mathbf{q}_u^e : \Gamma\left(\mathbf{q}_u; \mathbf{v}^{\text{ext}}\right) = \mathbf{0}, \dot{\mathbf{q}}_u = \ddot{\mathbf{q}}_u = \mathbf{0} \right\}, \tag{4}$$

where $\Gamma(q_u; v^{\text{ext}}) = D_{uu}\ddot{q}_u + D_{ua}v^{\text{ext}} + H_u$.

To stabilize q_u onto \mathcal{E} , we update q_a motion to incorporate balance control as

$$\boldsymbol{v}^{\text{int}} = -\boldsymbol{D}_{ua}^{+}(\boldsymbol{H}_{u} + \boldsymbol{D}_{uu}\boldsymbol{v}_{u}^{\text{int}}), \tag{5}$$

where $D_{ua}^+ = (D_{ua}^T D_{ua})^{-1} D_{ua}^T$ denotes the generalized inverse of D_{ua} . $v_u^{\rm int}$ is the auxiliary control that drives error $e_u = q_u - q_u^e$ towards zero. The final control is obtained by replacing $v^{\rm ext}$ in (3) with $v^{\rm int}$, that is,

$$\boldsymbol{u}^{\mathrm{int}} = \boldsymbol{D}_{aa} \boldsymbol{v}^{\mathrm{int}} + \boldsymbol{D}_{au} \ddot{\boldsymbol{q}}_{u} + \boldsymbol{H}_{a}. \tag{6}$$

The above EIC-based control achieves trajectory tracking for S_a and balance for S_u simultaneously [9], [23]. It has been shown in [9] that with an assumption that the robot model errors are affine with tracking errors, the control $u^{\rm int}$ guarantees both e_a and e_u convergence to a neighborhood of the origin exponentially.

B. Limitations of the EIC-based Control

In this subsection, we show the limitations of the above EIC-based control design. The limitation comes from (5)

that uses a mapping from low-dimensional (m) to high-dimensional (n) space. For robot control (6), it has been shown that there exists a finite time T>0 and for small number $\epsilon>0$, $\|{\bf q}_u(t)-{\bf q}_u^e(t)\|<\epsilon$ for t>T [9]. Given the negligible error, we obtain ${\bf D}_{au}({\bf q}_a,{\bf q}_u)\approx {\bf D}_{au}({\bf q}_a,{\bf q}_u^e)$. We apply singular value decomposition to ${\bf D}_{ua}$ and ${\bf D}_{ua}^+$,

$$D_{ua} = U\Lambda V^T, \quad D_{ua}^+ = V\Lambda^+ U^T, \tag{7}$$

where $U \in \mathbb{R}^{m \times m}$ and $V \in \mathbb{R}^{n \times n}$ are unitary orthogonal matrices. $\Lambda = [\Lambda_m \ 0] \in \mathbb{R}^{m \times n}$ and $\Lambda^+ = [\Lambda_m^{-1} \ 0]^T \in \mathbb{R}^{n \times m}$ and $\Lambda_m = \operatorname{diag}(\sigma_1, ..., \sigma_m)$ with all singular values $0 < \sigma_1 \le \sigma_2 \le \cdots \le \sigma_m$.

Since V is a unitary orthogonal matrix, its column vectors serve as a set of complete bases in \mathbb{R}^n . Rewriting the q_a and v^{ext} in span(V), we have transformations

$$p_a = V^T q_a, \quad \nu^{\text{ext}} = V^T v^{\text{ext}},$$
 (8)

where $\boldsymbol{\nu}^{\mathrm{ext}} = [(\boldsymbol{\nu}_{m}^{\mathrm{ext}})^{T} \ (\boldsymbol{\nu}_{n}^{\mathrm{ext}})^{T}]^{T}$. Note that $[\boldsymbol{p}_{a}^{T} \ \boldsymbol{q}_{u}^{T}]^{T}$ still serves as a complete set of generalized coordinates for \mathcal{S} . The robot dynamics \mathcal{S}_{u} under control $\boldsymbol{u}^{\mathrm{ext}}$ is $\ddot{\boldsymbol{q}}_{u} = -\boldsymbol{D}_{uu}^{-1}(\boldsymbol{D}_{ua}\boldsymbol{v}^{\mathrm{ext}} + \boldsymbol{H}_{u})$. Plugging (7) and (8) into the above dynamics yields

$$\ddot{q}_u = -D_{uu}^{-1}(U\Lambda\nu_m^{\text{ext}} + H_u). \tag{9}$$

For \mathcal{E} , q_u^e is obtained by solving $\Gamma_0(q_u; v^{\mathrm{ext}}) = \mathbf{0}$. With the above discussion, we substitute $\bar{D}_{ua}(q_u^e)$ with $\bar{D}_{ua}(q_u)$ in Γ_0 and therefore, using (7), $\Gamma_0 = \mathbf{0}$ is rewritten into

$$\left. \Lambda \boldsymbol{\nu}_{m}^{\text{ext}} + \boldsymbol{U}^{T} \boldsymbol{H}_{u}^{gp} \right|_{\boldsymbol{q}_{u} = \boldsymbol{q}_{u}^{e}, \dot{\boldsymbol{q}}_{u} = \ddot{\boldsymbol{q}}_{u} = \boldsymbol{0}} = \boldsymbol{0}.$$
 (10)

The BEM \mathcal{E} only depends on $\nu_m^{\rm ext}$, which is in the subspace $\mathrm{span}\{V_1,...,V_m\}$ of V. The control effect $\nu_n^{\rm ext}$ in the subspace $\ker(D_{ua})$ is disposable when obtaining the BEM.

The control v^{int} in (5) is augmented by matrix D_{ua}^+ using v_u^{int} , which is a map from a low- to high-dimensional space. We substitute (7) into (5) and the motion of \mathcal{S}_a under control v_u^{int} becomes

$$\ddot{q}_a = v^{\text{int}} = -V\Lambda^+ U^T \left(H_u + \bar{D}_u v_u^{\text{int}} \right). \tag{11}$$

We rewrite the above equation in the new coordinate p_a and under the EIC-based control, the closed-loop of S becomes

$$\ddot{p}_{ai} = -\frac{\boldsymbol{U}_{i}^{T} \left(\boldsymbol{H}_{u} + \boldsymbol{D}_{uu} \boldsymbol{v}_{u}^{\mathrm{int}}\right)}{\sigma_{i}}, \ i = 1, ..., m,$$
 (12a)

$$\ddot{p}_{a(m+j)} = 0, \ j = 1, ..., n - m, \tag{12b}$$

$$\ddot{q}_u = v_u^{\text{int}}. ag{12c}$$

Obviously, no control appears for coordinates in $\ker(D_{ua})$ as shown by (12b) and only m actuated coordinates in $\operatorname{span}(V)$ are under active control; see (12a). The designed control steers only a part of the generalized coordinates and the other part is without control.

With the above-revealed limitation of the EIC-based control and considering the data-driven model for robot dynamics, this work mainly focuses on the following problem.

Problem statement: The goal of robot control is to design an enhanced EIC-based control to drive the q_a to follow a given profile q_a^d and simultaneously q_u to be stabilized on the estimated \mathcal{E} using the GP-based data-driven model.

III. GP-BASED ROBOT DYNAMICS MODEL

In this section, we present a GP-based dynamics model. The enhanced EIC-based control design in the next section will be built on a selected nominal model.

A. GP-Based Robot Model

We consider to capture the robot dynamics using a GP-based data-driven method. We consider a multivariate continuously smooth function y=f(x)+w, where w is the zero-mean Gaussian noise. Denote the training data sampled from y=f(x)+w is $\mathbb{D}=\{X,Y\}=\{x_i,y_i\}_{i=1}^N$, where $X=\{x_i\}_{i=1}^N$, $Y=\{y_i\}_{i=1}^N$, $x_i\in\mathbb{R}^{n_x}$, and $N\in\mathbb{N}$ is the number of the data point. The GP model is trained by maximizing posterior probability $p(Y;X,\alpha)$ over the hyperparameters α . That is, α is obtained by solving

$$\min_{\pmb{\alpha}} - \log(\pmb{Y}; \pmb{X}, \pmb{\alpha}) = \min_{\pmb{\alpha}} - \frac{1}{2} \pmb{Y}^T \pmb{K}^{-1} \pmb{Y} - \frac{1}{2} \log \det(\pmb{K}),$$

where $\boldsymbol{K} = (K_{ij}), K_{ij} = k(\boldsymbol{x}_i, \boldsymbol{x}_j) = \sigma_f^2 \exp(-\frac{1}{2}(\boldsymbol{x}_i - \boldsymbol{x}_j)^T \boldsymbol{W}(\boldsymbol{x}_i - \boldsymbol{x}_j)) + \vartheta^2 \delta_{ij}, \boldsymbol{W} = \operatorname{diag}\{W_1, \cdots, W_{n_x}\} > 0, \delta_{ij} = 1 \text{ for } i = j, \text{ and } \boldsymbol{\alpha} = \{\boldsymbol{W}, \sigma_f, \vartheta^2\} \text{ are parameters.}$

Given a new x^* , the GP model predicts the corresponding y and the joint distribution is

$$\begin{bmatrix} \mathbf{Y} \\ y \end{bmatrix} \sim \mathcal{N} \left(\mathbf{0}, \begin{bmatrix} \mathbf{K} & \mathbf{k}^T \\ \mathbf{k} & k^* \end{bmatrix} \right), \tag{13}$$

where $k = k(x^*, X)$ and $k^* = k(x^*, x^*)$. The mean value and variance for input x^* are

$$\mu_i(\mathbf{x}^*) = \mathbf{k}^T \mathbf{K}^{-1} \mathbf{Y}, \ \Sigma_i(\mathbf{x}^*) = k^* - \mathbf{k} \mathbf{K}^{-1} \mathbf{k}^T.$$
 (14)

To apply the GP model for robot dynamics \mathcal{S} , we first build a nominal model

$$S^n: \bar{D}\ddot{q} + \bar{H} = u, \tag{15}$$

where \bar{D} and \bar{H} are the nominal inertia and nonlinear matrices, respectively. In general, the nominal dynamics equation does not hold for the data sampled from physical robot systems. The GP models are built to capture the difference between S^n and S. The dynamics model difference is

$$oldsymbol{H}^e = oldsymbol{D}\ddot{oldsymbol{q}} + oldsymbol{H} - ar{oldsymbol{D}}\ddot{oldsymbol{q}} - ar{oldsymbol{H}} = oldsymbol{u} - ar{oldsymbol{D}}\ddot{oldsymbol{q}} - ar{oldsymbol{H}}$$
 .

We build the GP models to capture $\boldsymbol{H}^e = [(\boldsymbol{H}_a^e)^T \ (\boldsymbol{H}_u^e)^T]^T$. Two GP models are used to predict \boldsymbol{H}_a^e and \boldsymbol{H}_u^e . The training data $\mathbb{D} = \{\boldsymbol{X}, \boldsymbol{Y}\}$ are sampled from \mathcal{S} as $\boldsymbol{X} = \{\boldsymbol{x}_i\}_{i=1}^N$, $\boldsymbol{Y} = \{\boldsymbol{H}_i^e\}_{i=1}^N$, where $\boldsymbol{x} = \{\boldsymbol{q}, \, \dot{\boldsymbol{q}}, \, \ddot{\boldsymbol{q}}\}$.

The GP predicted mean and variance are denoted as $(\boldsymbol{\mu}_i(\boldsymbol{x}), \boldsymbol{\Sigma}_i(\boldsymbol{x}))$ for \boldsymbol{H}_i^e , i=a,u. The GP-based robot dynamics model \mathcal{S}^{gp} is then given as

$$S_a^{gp}: \bar{D}_{aa}\ddot{q}_a + \bar{D}_{au}\ddot{q}_u + H_a^{gp} = u, \qquad (16a)$$

$$S_u^{gp}: \bar{D}_{ua}\ddot{q}_a + \bar{D}_{uu}\ddot{q}_u + H_u^{gp} = 0, \tag{16b}$$

where $H_i^{gp} = \bar{H}_i + \mu_i(x)$, i = a, u. The GP-based model prediction error is

$$\Delta = \begin{bmatrix} \Delta_a \\ \Delta_u \end{bmatrix} = \begin{bmatrix} \mu_a(x) - H_a^e \\ \mu_u(x) - H_u^e \end{bmatrix}. \tag{17}$$

To quantify the GP-based model prediction, we use Theorem 6 in [27] and obtain the following property for Δ .

Lemma 1: Given the training dataset \mathbb{D} , if the kernel function $k(\boldsymbol{x}_i, \boldsymbol{x}_j)$ is chosen such that \boldsymbol{H}_a^e for \mathcal{S}_a has a finite reproducing kernel Hilbert space norm $\|\boldsymbol{H}_a^e\|_k < \infty$, for given $0 < \eta_a < 1$,

$$\Pr\left\{\|\boldsymbol{\Delta}_{a}\| \leq \left\|\boldsymbol{\kappa}_{a}^{T}\boldsymbol{\Sigma}_{a}^{\frac{1}{2}}(\boldsymbol{x})\right\|\right\} \geq \eta_{a},\tag{18}$$

where $\Pr\{\cdot\}$ denotes the probability of an event, $\kappa_a \in \mathbb{R}^n$ and its i-th entry is $\kappa_{ai} = \sqrt{2\|\boldsymbol{H}_{a,i}^e\|_k^2 + 300\varsigma_i\ln^3\frac{N+1}{1-\eta_a^{\frac{1}{\alpha}}}},$ $\varsigma_i = \max_{\boldsymbol{x},\boldsymbol{x}'\in\boldsymbol{X}}\frac{1}{2}\ln|1+\vartheta_i^{-2}k_i\left(\boldsymbol{x},\boldsymbol{x}'\right)|.$ A similar conclusion holds for Δ_u with probability $0<\eta_u<1$.

B. Nominal Model Selection

With the constructed GP models, the next goal is to develop an enhanced EIC-based control to achieve stability and performance by eliminating the limitations that were discussed in the previous section. To achieve such a goal, we first require bounded matrices \bar{D} and \bar{H} . Inverting inertia matrix \bar{D} is required for feedback linearization and thus, \bar{D} is selected invertible. Second, the uncontrolled motion exists in the kernel of matrix \bar{D}_{ua} . If $\ker(\bar{D}_{ua})$ is constant, the uncontrolled motion appears in the fixed subspace of the configuration space. Therefore, it is required that the kernel of \bar{D}_{ua} is non-constant. As mentioned previously, the uncontrolled motion happens due to controller updating from the low- to high-dimensional spaces. If the unactuated coordinates depend on m (out of n) control inputs, we only need to update this m-input set.

From the above reasoning, we obtain the following conditions for the nominal model.

- \mathcal{C}_1 : $\bar{D} = \bar{D}^T \succ 0$, i.e., positive definite, $\|\bar{D}\| \le d$, $\|\bar{H}\| \le h$, where constants $0 < d, h < \infty$;
- \mathcal{C}_2 : $\operatorname{rank}(\bar{\mathbf{D}}_{aa}) = n$, $\operatorname{rank}(\bar{\mathbf{D}}_{uu}) = \operatorname{rank}(\bar{\mathbf{D}}_{ua}) = m$;
- C_3 : non-constant kernel of D_{ua} ;
- C_4 : motion of the unactuated coordinates depend on only m control inputs.

We will illustrate how to select nominal models that satisfy the above conditions in Section V.

IV. GP-ENHANCED EIC-BASED CONTROL

In this section, we first present the partial EIC (PEIC) control that takes advantage of the GP predictive model and explicitly eliminates uncontrolled motion. Stability and performance analysis are then discussed.

A. PEIC-Based Control Design

With GP predictive models S^{gp} , we incorporate the predictive variance of S_a^{gp} into the auxiliary control v^{ext} as

$$\hat{\mathbf{v}}^{\text{ext}} = \ddot{\mathbf{q}}_a^d - \mathbf{k}_{p1}(\mathbf{\Sigma}_a)\mathbf{e}_a - \mathbf{k}_{d1}(\mathbf{\Sigma}_a)\dot{\mathbf{e}}_a \tag{19}$$

where $k_{p1}(\Sigma_a), k_{d1}(\Sigma_a) \succ 0$ are control gains that depend on variance Σ_a . Given the GP-based dynamics, the BEM is estimated by solving the optimization problem

$$\hat{\mathbf{q}}_u^e = \arg\min_{\mathbf{q}_u} \|\mathbf{\Gamma}(\mathbf{q}_u; \hat{\mathbf{v}}^{\text{ext}})\|. \tag{20}$$

The updated control design is

$$\hat{\boldsymbol{v}}_u^{\text{int}} = \ddot{\hat{\boldsymbol{q}}}_u^e - \boldsymbol{k}_{p2}(\boldsymbol{\Sigma}_u)\hat{\boldsymbol{e}}_u - \boldsymbol{k}_{d2}(\boldsymbol{\Sigma}_u)\dot{\hat{\boldsymbol{e}}}_u, \tag{21}$$

where $\hat{e}_u = q_u - \hat{q}_u^e$ is the internal system tracking error relative to the estimated BEM. $k_{p2}(\Sigma_u), k_{d2}(\Sigma_u) \succ 0$ are also designed and tuned by the estimated GP variance Σ_u .

Let $\Delta q_u^e = q_u^e - \hat{q}_u^e$ denote the BEM estimation error and the actual BEM is $q_u^e = \hat{q}_u^e + \Delta q_u^e$. The control design based on the actual BEM is $v_u^{\text{int}} = \ddot{q}_u^e - k_{p2}(\Sigma_u)e_u - k_{d2}(\Sigma_u)e_u$ and therefore, we have

$$\boldsymbol{v}_{u}^{\mathrm{int}} = \hat{\boldsymbol{v}}_{u}^{\mathrm{int}} - \Delta \boldsymbol{v}_{u}^{\mathrm{int}}$$

where $\Delta v_u^{\rm int} = \Delta \ddot{q}_u^e + k_{p2} \Delta q_u^e + k_{d2} \Delta \dot{q}_u^e$. Compared to (4), the BEM estimation error comes from GP modeling error and optimization accuracy. It is reasonable to assume that Δq_u^e is bounded. Because of the bounded Gaussian kernel function, the GP prediction variances are also bounded, i.e.,

$$\|\mathbf{\Sigma}_a(\mathbf{x})\| \le (\sigma_a^{\max})^2, \|\mathbf{\Sigma}_u(\mathbf{x})\| \le (\sigma_u^{\max})^2,$$
 (22)

where $\sigma_a^{\max} = \max_i (\sigma_{f_{ai}}^2 + \vartheta_{ai}^2)^{1/2}$, $\sigma_u^{\max} = \max_i (\sigma_{f_{ui}}^2 + \vartheta_{ui}^2)^{1/2}$, σ_f and ϑ are the hyperparameters in each channel. Furthermore, we require the control gains to satisfy the following bounds

$$k_{i1} \le \lambda(\mathbf{k}_{i1}) \le k_{i3}, \quad k_{i2} \le \lambda(\mathbf{k}_{i2}) \le k_{i4}, \ i = p, d,$$

for constants $k_{pj}, k_{dj} > 0, j = 1, \dots, 4$, where $\lambda(\cdot)$ denotes the eigenvalue operator.

The control design v^{int} in (5) revises the preliminary control v^{ext} . Under the updated control, q_a serves as a control input to drive q_u to q_u^e . For the PEIC-based control, we instead consider a partial coupling constraint between q_a and q_u and assign m control inputs (equivalently the actuated coordinates) for unactuated subsystem control. To achieve such a goal, we partition the actuated coordinates as $q_a = [q_{aa}^T \ q_{au}^T]^T$, $q_{au} \in \mathbb{R}^m$, $q_{aa} \in \mathbb{R}^{n-m}$, and $u = [u_a^T \ u_u^T]^T$. The \mathcal{S}^{gp} dynamics in (16) is rewritten as

$$\begin{bmatrix} \bar{D}_{aa}^{a} & \bar{D}_{aa}^{au} & \bar{D}_{au}^{a} \\ \bar{D}_{aa}^{ua} & \bar{D}_{aa}^{u} & \bar{D}_{au}^{u} \\ \bar{D}_{ua}^{a} & \bar{D}_{ua}^{u} & \bar{D}_{uu}^{u} \end{bmatrix} \begin{bmatrix} \ddot{q}_{aa} \\ \ddot{q}_{au} \\ \ddot{q}_{u} \end{bmatrix} + \begin{bmatrix} H_{aa}^{gp} \\ H_{au}^{gp} \\ H_{u}^{gp} \end{bmatrix} = \begin{bmatrix} u_{a} \\ u_{u} \\ 0 \end{bmatrix}, (23)$$

where all block matrices are in proper dimension. We rewrite (23) into three groups as

$$S_{aa}^{gp}: \bar{D}_{aa}^{a}\ddot{q}_{aa} + H_{aa}^{a} = u_{a}, \tag{24a}$$

$$S_{au}^{gp}: \bar{D}_{aa}^{u}\ddot{q}_{au} + \bar{D}_{au}^{u}\ddot{q}_{u} + H_{au}^{u} = u_{u}, \tag{24b}$$

$$S_u^{gp}: \bar{D}_{ua}^u \ddot{q}_{au} + \bar{D}_{uu} \ddot{q}_u + H_{un} = 0, \tag{24c}$$

where $\boldsymbol{H}_{an}^{aa} = \bar{\boldsymbol{D}}_{aa}^{au}\ddot{q}_{au} + \bar{\boldsymbol{D}}_{au}^{a}\ddot{q}_{u} + \boldsymbol{H}_{aa}^{gp}, \ \boldsymbol{H}_{an}^{u} = \bar{\boldsymbol{D}}_{aa}^{ua}\ddot{q}_{aa} + \bar{\boldsymbol{D}}_{au}^{u}\ddot{q}_{u} + \boldsymbol{H}_{au}^{gp}, \ \text{and} \ \boldsymbol{H}_{un} = \bar{\boldsymbol{D}}_{ua}^{a}\ddot{q}_{aa} + \boldsymbol{H}_{u}^{gp}.$ Apparently, \mathcal{S}_{u}^{gp} is virtually independent of \mathcal{S}_{aa}^{gp} , since there is "no dynamics coupling". The dynamics coupling virtually exists only between \mathcal{S}_{u}^{gp} and \mathcal{S}_{au}^{gp} .

Let control \hat{v}^{ext} in (19) be partitioned into \hat{v}^{ext}_a and \hat{v}^{ext}_u , corresponding to q_{aa} and q_{au} , respectively. \hat{v}^{ext}_a is directly applied to \mathcal{S}^{gp} and \hat{v}^{ext}_u is updated for balance control purpose. As aforementioned, the necessary conditions to eliminate the uncontrolled motion in \mathcal{S}_a is that q_u only

depends on m inputs. The task of driving q_u to q_u^e is assigned to q_{au} coordinates only. With this observation, the PEIC-based control is given as $\hat{\boldsymbol{u}}^{\text{int}} = [\hat{\boldsymbol{u}}_a^T \ \hat{\boldsymbol{u}}_u^T]^T$ with

$$\hat{u}_{a} = \bar{D}_{aa}^{a} \hat{v}_{a}^{\text{ext}} + H_{an}^{a}, \hat{u}_{u} = \bar{D}_{aa}^{u} \hat{v}^{\text{int}} + \bar{D}_{au}^{u} \ddot{q}_{u} + H_{an}^{u},$$
(25)

where $\hat{v}^{\text{int}} = -(\bar{D}_{ua}^u)^{-1}(H_{un} + \bar{D}_{uu}\hat{v}_u^{\text{int}})$. The auxiliary controls are \hat{v}_a^{ext} and \hat{v}_u^{int} . The unactuated subsystem only depends on u_u under the PEIC design. Fig. 1 illustrates the overall flowchart of the PEIC-based control design.

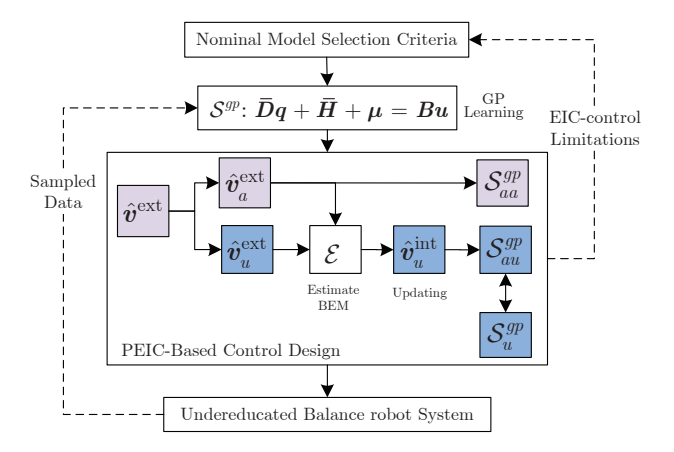


Fig. 1. An overall flowchart of the PEIC-based control design.

B. Stability and Performance Analysis

To investigate the closed-loop dynamics, we take the GP prediction error and the BEM estimation error into consideration. The GP prediction error in (17) is extended to Δ_{aa} , Δ_{au} and Δ_{u} for q_{aa} , q_{au} , q_{u} dynamics, respectively. Under the PEIC-based control, the dynamics of S becomes

$$\begin{split} \ddot{q}_{aa} &= \hat{v}_{a}^{\text{ext}} - (\bar{D}_{aa}^{a})^{-1} \Delta_{aa}, \\ \ddot{q}_{au} &= -(\bar{D}_{ua}^{u})^{-1} (H_{un} + \bar{D}_{uu} \hat{v}_{u}^{\text{int}}) - (\bar{D}_{aa}^{u})^{-1} \Delta_{au}, \\ \ddot{q}_{u} &= \hat{v}_{u}^{\text{int}} - \bar{D}_{uu}^{-1} [\Delta_{u} - \bar{D}_{ua}^{u} (\bar{D}_{aa}^{u})^{-1} \Delta_{au}]. \end{split}$$

The BEM obtained by (20) under input $[\ddot{q}_{aa} \ \hat{v}_u^{\text{ext}}]$ is equivalent to inverting (24c), that is,

$$\left.\hat{oldsymbol{v}}_{u}^{ ext{ext}}=-\left(ar{oldsymbol{D}}_{ua}^{u}
ight)^{-1}oldsymbol{H}_{un}
ight|_{oldsymbol{q}_{u}=\hat{oldsymbol{q}}_{u}^{e},\dot{oldsymbol{q}}_{u}=\ddot{oldsymbol{q}}_{u}=oldsymbol{0}}.$$

Substituting the above equation into the q_{au} dynamics yields $\ddot{q}_{au} = \hat{v}_u^{\rm ext} + O_{au}$, where $O_{au} = -(\bar{D}_{ua}^u)^{-1}\bar{D}_{uu}\hat{v}_u^{\rm int} - (\bar{D}_{ua}^u)^{-1}\Delta_{au} + O_{\rm hot}$ and $O_{\rm hot}$ denotes the higher order terms.

Defining the total error $e_q = [e_a^T \ e_u^T]^T$ and $e = [e_q^T \ \dot{e}_q^T]^T$, the closed-loop error dynamics becomes

$$\dot{e} = \begin{bmatrix} \dot{e}_q \\ \ddot{e}_q \end{bmatrix} = \underbrace{\begin{bmatrix} \mathbf{0} & I_{n+m} \\ -\mathbf{k}_p & -\mathbf{k}_d \end{bmatrix}}_{A} \begin{bmatrix} e_q \\ \dot{e}_q \end{bmatrix} + \underbrace{\begin{bmatrix} \mathbf{0} \\ O_{\text{tot}} \end{bmatrix}}_{O} = Ae + O \quad (26)$$

with
$$O_{ ext{tot}} = [O_a^T \ O_u^T]^T, \ O_a = [O_{aa}^T \ O_{au}^T]^T, \ O_{aa} = -(\bar{D}_{aa}^a)^{-1} \Delta_{aa}, \ O_u = -\bar{D}_{uu}^{-1} (\Delta_u - \bar{D}_{uu}^u (\bar{D}_{aa}^u)^{-1} \Delta_{au}) - \Delta v_u^{ ext{int}}, \ k_p = \operatorname{diag}(k_{p1}, k_{p2}), \ \operatorname{and} \ k_d = \operatorname{diag}(k_{d1}, k_{d2}).$$

Because of bounded \bar{D} , there exists constants $0 < d_{a1}, d_{a2}, d_{u1}, d_{u2} < \infty$ such that $d_{a1} \le \|\bar{D}_{aa}\| \le d_{a2}$ and

 $d_{u1} \leq \|\bar{D}_{uu}\| \leq d_{u2}$. The perturbation terms are further expressed and bounded as

$$\begin{aligned} \|\boldsymbol{O}_a\| &= \left\| - \begin{bmatrix} \boldsymbol{0} \\ (\bar{\boldsymbol{D}}_{ua}^u)^{-1} \bar{\boldsymbol{D}}_{uu} \hat{\boldsymbol{v}}_u^{\text{int}} \end{bmatrix} - (\bar{\boldsymbol{D}}_{aa}^a)^{-1} \boldsymbol{\Delta}_a + \begin{bmatrix} \boldsymbol{0} \\ \boldsymbol{O}_{\text{hot}} \end{bmatrix} \right\| \\ &\leq \frac{d_{u2}}{\sigma_*} \left\| \hat{\boldsymbol{v}}_u^{\text{int}} \right\| + \frac{1}{d_{-1}} \left\| \boldsymbol{\Delta}_a \right\| + \left\| \boldsymbol{O}_{\text{hot}} \right\| \end{aligned}$$

and

$$\begin{aligned} \|\boldsymbol{O}_{u}\| &= \left\| -\bar{\boldsymbol{D}}_{uu}^{-1} (\boldsymbol{\Delta}_{u} - \bar{\boldsymbol{D}}_{ua}^{u} (\bar{\boldsymbol{D}}_{aa}^{u})^{-1} \boldsymbol{\Delta}_{au}) - \Delta \boldsymbol{v}_{u}^{\text{int}} \right\| \\ &\leq \frac{1}{d_{v1}} \left\| \boldsymbol{\Delta}_{u} \right\| + \frac{\sigma_{m}}{d_{v1} d_{v1}} \left\| \boldsymbol{\Delta}_{a} \right\| + \left\| \boldsymbol{\Delta} \boldsymbol{v}_{u}^{\text{int}} \right\|. \end{aligned}$$

The perturbation O_{hot} is due to approximation and Δv_u^{int} is the control difference due to the BEM calculation by the GP prediction, and we assume they are affine functions with total error e, that is,

$$\|O_{\text{hot}}\| \le c_1 \|e\| + c_2, \quad \|\Delta v_u^{\text{int}}\| \le c_3 \|e\| + c_4$$

with $0 < c_i < \infty$, $i = 1, \cdots, 4$. From (22), we have $\|\boldsymbol{\kappa}_a^T \boldsymbol{\Sigma}_a^{\frac{1}{2}}\| \leq \sigma_a^{\max} \|\boldsymbol{\kappa}_a\|$ and $\|\boldsymbol{\kappa}_u^T \boldsymbol{\Sigma}_u^{\frac{1}{2}}\| \leq \sigma_u^{\max} \|\boldsymbol{\kappa}_u\|$. Thus, for $0 < \eta < 1$, we can show that

$$\Pr\{\|\boldsymbol{O}\| \le d_1 + d_2 \|\boldsymbol{e}\| + l_u \|\boldsymbol{\kappa}_u\| + l_a \|\boldsymbol{\kappa}_a\|\} \ge \eta,$$

with
$$\eta=\eta_a\eta_u$$
, $d_1=c_2+(1+\frac{d_{u2}}{\sigma_1})c_4$, $d_2=c_1+\frac{d_{u2}}{\sigma_1}c_3$, $l_a=\frac{\sigma_a^{\max}(d_{u1}+\sigma_m)}{d_{u1}d_{a1}}$, $l_u=\frac{\sigma_u^{\max}}{d_{u1}}$. With the above results, we have the following results about

With the above results, we have the following results about the stability and performance of the PEIC-based control and the proof is neglected due to page limit. The detailed proof can be found in the extended version of the paper [28].

Lemma 2: For robot dynamics (2), using the GP-based model (16) and under the PEIC-based control design (19), (21) and (25), the system error *e* exponentially converges to a small ball near the origin.

V. EXPERIMENTAL RESULTS

We used two inverted pendulum platforms to conduct experiments to validate and demonstrate the robot control design. Fig. 2(a) shows a 2-DOF rotary inverted pendulum and Fig. 2(b) for a 3-DOF robotic leg that has an inverted link as the controlled balance task.

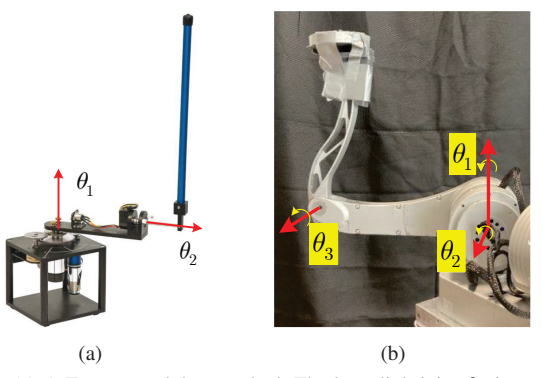


Fig. 2. (a) A Furuta pendulum testbed. The base link joint θ_1 is actuated and the pendulum link joint θ_2 is unactuated. (b) A three-link robotic leg with two base links θ_1 and θ_2 are actuated and the top link θ_3 is unactuated.

The rotary inverted pendulum (2 DOFs, n=m=1) was made by Quanser Inc. and we used this platform to

illustrate the EIC-based control. The base joint (θ_1) was actuated by a DC motor and the inverted pendulum joint (θ_2) was unactuated. The physical model in (2) is given in [29]. The control input is motor voltage. Since the condition \mathcal{C}_4 is satisfied automatically, there is no uncontrolled motion if the EIC-based control is applied. Either a constant nominal model or a time-varying nominal model should work. We take the nominal models

$$\begin{split} \mathcal{S}^{n1}: \ \bar{\boldsymbol{D}}_{1} &= \frac{1}{100} \begin{bmatrix} 5 & -2 \, c_{2} \\ -2 \, c_{2} & 2 \end{bmatrix}, \ \bar{\boldsymbol{H}}_{1} = \begin{bmatrix} 0 \\ -\, s_{2} \end{bmatrix}, \\ \mathcal{S}^{n2}: \ \bar{\boldsymbol{D}}_{2} &= \frac{1}{100} \begin{bmatrix} 2 & 1 \\ 1 & 2 \end{bmatrix}, \ \bar{\boldsymbol{H}}_{2} &= \boldsymbol{0}, \end{split}$$

where $c_i = \cos\theta_i$, $s_i = \sin\theta_i$ for angle θ_i , i = 1, 2. The control gains $k_{p1} = 10 + 50\Sigma_a$, $k_{d1} = 3 + 10\Sigma_a$, $k_{p2} = 1000 + 500\Sigma_u$, and $k_{d2} = 100 + 200\Sigma_u$ were chosen. The reference trajectory was $\theta_1 = 0.5 \sin t + 0.3 \sin 1.5t$ rad. The control was implemented at 400 Hz in Matlab/Simulink real-time system. For comparison purposes, we also implemented a physical model-based EIC controller.

TABLE I Tracking Errors of Rotatory Inverted Pendulum

		\mathcal{S}^{n1}	\mathcal{S}^{n2}	Model-Based
ĺ	$ e_1 $ (rad)	0.024 ± 0.017	0.081 ± 0.105	0.109 ± 0.040
	$ e_2 $ (rad)	0.009 ± 0.005	0.009 ± 0.008	0.026 ± 0.015

Fig. 3 shows the experimental results. With either S^{n1} or S^{n2} , the base link closely follows the reference trajectory and a similar trend is found for the pendulum motion (see Fig. 3(b)). However, the tracking error was reduced and the pendulum closely followed the small vibrations for S^{n1} . With S^{n2} , the tracking errors became large when the base link changed rotation direction; see Fig. 3(c) at t = 10, 17, 22 s. Since condition C_4 is automatically satisfied, both nominal models worked for the learning and EIC-based control design. Table I lists the statistics of the tracking errors (i.e., mean and one standard deviation). For both subsystems, the errors with the learning-based approach are smaller. In particular, with a time-varying nominal model, the tracking error (mean value) for e_1 and e_2 reduced 75% and 65% respectively in comparison with those under the physical model. A relatively large error was with S^{n2} and this can be due to that a constant nominal model did not reflect the time-varying property of the robot dynamics.

We next use a 3-DOF robotic leg ($n=2,\ m=1$) to demonstrate the proposed control design. The control implementation was at 200 Hz through Robot Operating System (ROS). The nominal model was given by

$$\bar{\boldsymbol{D}} = \begin{bmatrix} 0.15 & 0.025 \, c_2 & 0.025 \, c_3 \\ 0.025 \, c_2 & 0.15 & 0.05 \, c_{23} \\ 0.025 \, c_3 & 0.05 \, c_{23} & 0.1 \end{bmatrix}, \ \bar{\boldsymbol{H}} = \begin{bmatrix} 0 \\ 0.2 \, c_2 \\ 0.1 \, s_3 \end{bmatrix},$$

where $c_{ij} = \cos(\theta_i - \theta_j)$. We applied an open-loop control (combination of sine wave torque) to excite the system and obtained the training data. The control gains were $k_{p1} = 15.0I_2 + 20\Sigma_a$, $k_{d1} = 3I_2 + 10\Sigma_a$, $k_{p2} = 25 + 20\Sigma_u$, $k_{d2} = 25 + 20\Sigma_u$

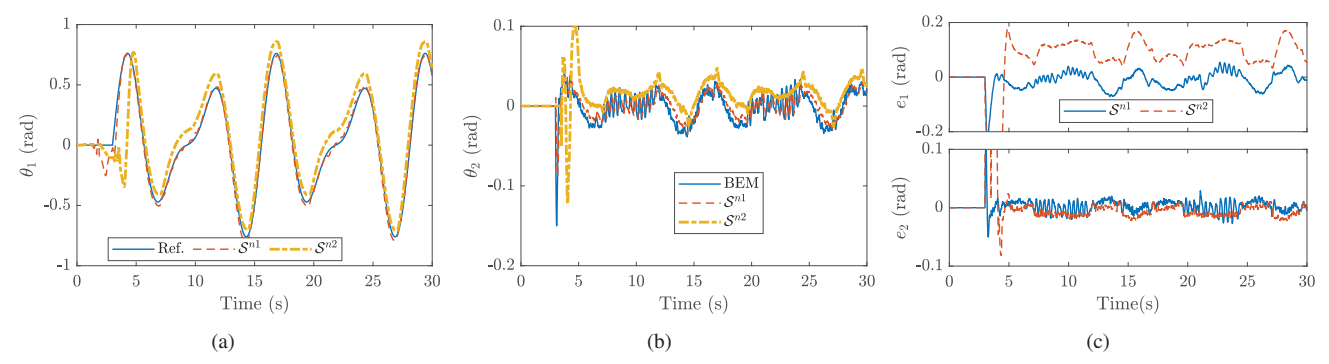


Fig. 3. Experiment results with rotary inverted pendulum (a) Arm rotation angles. (b) Pendulum rotation angles. (c) Tracking control errors.

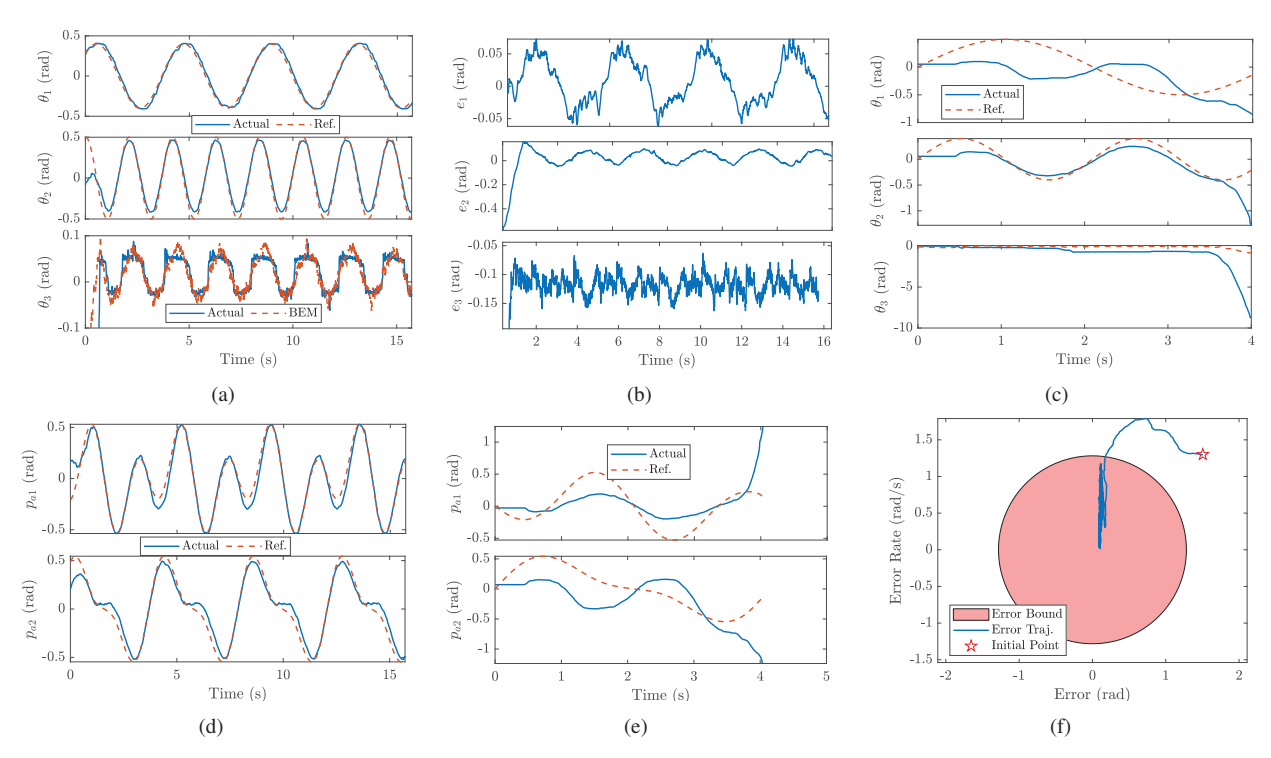


Fig. 4. Experiment results with the underactuated robotic leg. (a) Motion profiles and (b) tracking errors under the PEIC-based control. (c) Motion profiles under the EIC-based control. (d) Motion profiles in the new coordinate p_a under the PEIC-based control. (e) Motion profile p_a under the EIC-based control. (f) Error trajectory in the $\|e_a\|$ - $\|\dot{e}_a\|$ plane.

 $5.5 + 10\Sigma_u$. The reference trajectory was $\theta_1^d = 0.5 \sin t$, $\theta_2^d = 0.4 \sin 3t$ rad. We chose $q_{aa} = \theta_1$ and $q_{au} = \theta_2$.

Under the proposed control, the system followed the given reference trajectory closely and the third link was balanced around the BEM as shown in Fig. 4(a). In Fig. 4(b), the tracking error of joint θ_1 is between -0.05 to 0.05 rad, while the tracking error of joint θ_2 is between -0.1 to 0.1 rad. Fig. 4(c) shows the results under the regular EICbased control and it is clear that the system became unstable. The motion of the actuated coordinate in the new coordinate p_a is shown in Figs. 4(d) and 4(e) and p_{a2} represents the uncontrolled motion variable. Although p_{a1} followed the reference, the p_{a2} profile showed a large error due to the lack of control. Fig. 4(f) shows the estimated error bound and it is clear that the tracking error entered and remained inside the bounded area. The above results confirmed that the uncontrolled motion was eliminated and the simultaneously tracking and balance control property of EIC-based control

was preserved. To further improve the tracking performance, a large size of training data can be used with distributed GP agents to reduce the computational cost [20].

VI. CONCLUSION

This paper proposed a learning-based controller for underactuated balance robots. The proposed control was an extension of the external and internal convertible form control (i.e., EIC-based control). The EIC-based control aimed to achieve tracking and balance simultaneously. However, we showed that uncontrolled motion existed under the EIC-based control. We identified the conditions under which the uncontrolled motion happened and also proposed the GP-enhanced EIC-based control. The proposed new robot control preserved the structure property of the EIC-based control and achieved tracking and balance tasks. We demonstrated the new control design on two experimental platforms and confirmed that stability and balance were guaranteed.

REFERENCES

- [1] G. Turrisi, M. Capotondi, C. Gaz, V. Modugno, G. Oriolo, and A. D. Luca, "On-line learning for planning and control of underactuated robots with uncertain dynamics," *IEEE Robot. Automat. Lett.*, vol. 7, no. 1, pp. 358–365, 2022.
- [2] N. Kant and R. Mukherjee, "Orbital stabilization of underactuated systems using virtual holonomic constraints and impulse controlled poincaré maps," Syst. Contr. Lett., vol. 146, pp. 1–9, 2020, article 104813.
- [3] K. Chen, J. Yi, and D. Song, "Gaussian-process-based control of underactuated balance robots with guaranteed performance," *IEEE Trans. Robotics*, vol. 39, no. 1, pp. 572–589, 2023.
- [4] F. Han and J. Yi, "Stable learning-based tracking control of underactuated balance robots," *IEEE Robot. Automat. Lett.*, vol. 6, no. 2, pp. 1543–1550, 2021.
- [5] T. Beckers, D. Kulić, and S. Hirche, "Stable Gaussian process based tracking control of Euler–Lagrange systems," *Automatica*, vol. 103, pp. 390–397, 2019.
- [6] K. Chen and J. Yi, "On the relationship between manifold learning latent dynamics and zero dynamics for human bipedal walking," in *Proc. IEEE/RSJ Int. Conf. Intell. Robot. Syst.*, Hamburg, Germany, 2015, pp. 971–976.
- [7] J. W. Grizzle, C. Chevallereau, R. W. Sinnet, and A. D. Ames, "Models, feedback control, and open problems in 3D bipedal robotic walking," *Automatica*, vol. 50, pp. 1955–1988, 2014.
- [8] F. Han, X. Huang, Z. Wang, J. Yi, and T. Liu, "Autonomous bikebot control for crossing obstacles with assistive leg impulsive actuation," *IEEE/ASME Trans. Mechatronics*, vol. 27, no. 4, pp. 1882–1890, 2022.
- [9] N. Getz, "Dynamic inversion of nonlinear maps with applications to nonlinear control and robotics," Ph.D. dissertation, Dept. Electr. Eng. and Comp. Sci., Univ. Calif., Berkeley, CA, 1995.
- [10] M. Maggiore and L. Consolini, "Virtual holonomic constraints for euler-lagrange systems," *IEEE Trans. Automat. Contr.*, vol. 58, no. 4, pp. 1001–1008, 2013.
- [11] C. C. de Wit, B. Espiau, and C. Urrea, "Orbital stabilization of underactuated mechanical systems," *IFAC Proceedings Volumes*, vol. 35, no. 1, pp. 527–532, 2002, 15th IFAC World Congress.
- [12] E. R. Westervelt, J. W. Grizzle, and D. E. Koditschek, "Hybrid zero dynamics of planar biped walkers," *IEEE Trans. Automat. Contr.*, vol. 48, no. 1, pp. 42–56, 2003.
- [13] J. W. Grizzle, G. Abba, and F. Plestan, "Asymptotically stable walking for biped robots: Analysis via systems with impulse effects," *IEEE Trans. Automat. Contr.*, vol. 46, no. 1, pp. 51–64, 2001.
- [14] K. Åström and K. Furuta, "Swinging up a pendulum by energy control," *Automatica*, vol. 36, no. 2, pp. 287–295, 2000.
- [15] I. Fantoni and R. Lozano and M. W. Spong, "Energy based control of pendubot," *IEEE Trans. Automat. Contr.*, vol. 45, no. 4, pp. 725–729, 2000.
- [16] X. Xin and M. Kaneda, "Analysis of the energy-based control for swinging up two pendulums," *IEEE Trans. Automat. Contr.*, vol. 50, no. 5, pp. 679–684, 2005.
- [17] A. S. Shiriaev, J. W. Perram, and C. Canudas-de-Wit, "Constructive tool for orbital stabilization of underactuated nonlinear systems: Virtual constraints approach," *IEEE Trans. Automat. Contr.*, vol. 50, no. 8, pp. 1164–1176, 2005.
- [18] P. Wang, F. Han, and J. Yi, "Gyroscopic balancer-enhanced motion control of an autonomous bikebot," ASME J. Dyn. Syst., Meas., Control, vol. 145, no. 10, 2023, article 101002.
- [19] F. Han and J. Yi, "Safe motion control of autonomous vehicle ski-stunt maneuvers," *IEEE/ASME Trans. Mechatronics*, pp. 1–12, 2023.
- [20] A. Lederer, Z. Yang, J. Jiao, and S. Hirche, "Cooperative control of uncertain multiagent systems via distributed gaussian processes," *IEEE Trans. Automat. Contr.*, vol. 68, no. 5, pp. 3091–3098, 2023.
- [21] T. Beckers and S. Hirche, "Prediction with approximated gaussian process dynamical models," *IEEE Trans. Automat. Contr.*, vol. 67, no. 12, pp. 6460–6473, 2022.
- [22] M. Deisenroth and J. W. Ng, "Distributed gaussian processes," in *Proc. 32nd Int. Conf. Machine Learning*, F. Bach and D. Blei, Eds., vol. 37. PMLR, 2015, pp. 1481–1490.
- [23] F. Han and J. Yi, "On the learned balance manifold of underactuated balance robots," in *Proc. IEEE Int. Conf. Robot. Autom.*, London, UK, 2023, pp. 12254–12260.
- [24] M. K. Helwa, A. Heins, and A. P. Schoellig, "Provably robust learning-based approach for high-accuracy tracking control of lagrangian systems," *IEEE Robot. Automat. Lett.*, vol. 4, no. 2, pp. 1587–1594, 2019.

- [25] F. Han and J. Yi, "Cascaded nonlinear control design for highly underactuated balance robots," pp. 1–7, 2023, arXiv:2309.16805.
- [26] —, "Learning-based safe motion control of vehicle ski-stunt maneuvers," in *Proc. IEEE/ASME Int. Conf. Adv. Intelli. Mechatronics*, Sapporo, Japan, 2022, pp. 724–729.
- [27] N. Srinivas, A. Krause, S. M. Kakade, and M. W. Seeger, "Information-theoretic regret bounds for gaussian process optimization in the bandit setting," *IEEE Trans. Inform. Theory*, vol. 58, no. 5, pp. 3250–3265, 2012.
- [28] F. Han and J. Yi, "Gaussian process-based learning control of underactuated balance robots with an external and internal convertible modeling structure," arXiv preprint, pp. 1–14, 2023, arXiv:2312.10155.
- [29] J. Apkarian, P. Karam, and M. Levis, Instructor Workbook: Inverted Pendulum Experiment for Matlab/Simulink Users, Quanser Inc., Markham, Ontario, Canada, 2011.